Biochemistry

 Volume 40, Number 7 February 20, 2001

Current Topics

Reaction-Induced Infrared Difference Spectroscopy for the Study of Protein Reaction Mechanisms†

Christian Zscherp* and Andreas Barth*

Institut für Biophysik, Johann Wolfgang Goethe-Universität, Theodor-Stern-Kai 7, Haus 74, D-60590 Frankfurt am Main, Germany

Received November 7, 2000; Revised Manuscript Received December 28, 2000

ABSTRACT: This paper reviews state-of-the-art reaction-induced infrared difference spectroscopy of proteins. This technique enables detailed characterization of enzyme function on the level of single bonds of proteins, cofactors, or substrates. The following methods to initiate a reaction in the infrared sample are discussed: (i) light-induced difference spectroscopy, (ii) attenuated total reflection with buffer exchange, (iii) the infrared variant of stopped and continuous flow, (iv) temperature and pressure jump, (v) photolytical release of effector substances from caged compounds, (vi) equilibrium electrochemistry, and (vii) photoreduction. Illustrating applications are given including hot topics from the fields of bioenergetics, protein folding, and molecule−protein interaction.

Protein structure and function can be studied by various biochemical and biophysical approaches. Three-dimensional protein structures may be obtained by using X-ray crystallography, electron cryomicroscopy, or nuclear magnetic resonance. Unfortunately, these techniques are slow. On the other hand, methods provided with high time resolution often give less detail about structural features. Infrared spectroscopy (*1*) bridges this gap. It is able to supply rapid information about the backbone structure as well as about side chain conformation and environment on the level of individual groups (*1*−*8*). The potential of infrared spectroscopy fully unfolds when these two advantages—i.e., high structural information content and high time resolution—are used in combination. Thus, infrared spectroscopy is ideally suited to study the molecular mechanism of protein reactions.

The absorbance changes usually observed for protein reactions are very small, on the order of 0.1% of the total absorbance. In consequence, simply comparing the spectrum of a sample where the protein is in state A with a spectrum where it is in state B is successful only in favorable cases and for small proteins. In these cases the differences between the two states can be observed either by direct subtraction of the absorbance spectra of the two states or by analyzing the absorbance spectra using band-narrowing techniques such as second derivative techniques, Fourier self-deconvolution (*9*, *10*), and fine structure enhancement (*11*). However, in most cases it is advisable to trigger the transition between the two protein states of interest directly in the infrared cuvette. Combined with sensitive instrumentation, this approach allows the accurate detection of the subtle changes in the vibrational spectrum that accompany protein reactions. We review here the several options that are available for

† C.Z. acknowledges financial support from the Deutsche Forschungsgemeinschaft (Sonderforschungsbereiche 189 and 472). Part of the work of A.B. was funded by Grant Ma 1054/10-3 from the Deutsche Forschungsgemeinschaft. The present work is funded by Grants Ba 1887/1-1 and Ba 1887/2-1 from the Deutsche Forschungsgemeinschaft.

* Authors for correspondence. C.Z.: phone, +49 69 6301 6087; fax, +49 69 6301 5838; e-mail, zscherp@biophysik.uni-frankfurt.de. A.B.: phone, +49 69 6301 6087; fax, +49 69 6301 5838; e-mail, barth@biophysik.uni-frankfurt.de.

10.1021/bi002567y CCC: $20.00
Published on Web 01/25/2001

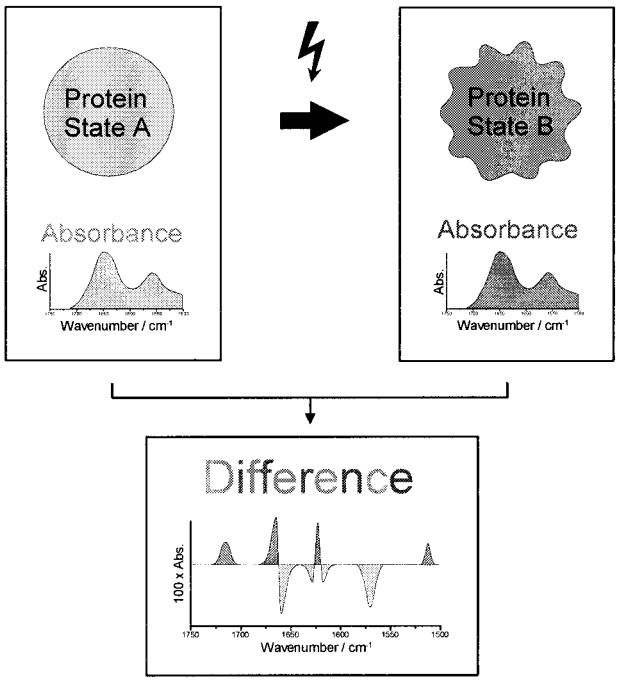

FIGURE 1: Principle of reaction-induced infrared difference spectroscopy. See text for further details.

reaction-induced infrared difference spectroscopy.

The Principle of Reaction-Induced Infrared Difference Spectroscopy. A typical infrared difference spectrum is generated as illustrated in Figure 1. The protein is prepared in a resting state A, and the absorbance of state A is recorded (Figure 1, left). Then the reaction is triggered, the protein proceeds to state B, and again the absorbance is recorded (Figure 1, right). Of course, state B may also be a sequence of several transient states. In that case the interconversion between the product states B_1, B_2, etc. can be followed by time-resolved methods (see below).

The small absorbance changes upon the transition from state A to state B are not obvious in the absorbance spectra. They are identified only when the difference between the two absorbance spectra is calculated and the scale is enlarged 100-fold (bottom). Shown is an idealized difference spectrum with the shading of the difference bands indicating that negative bands are characteristic of the initial state A and positive bands of the product state(s) B. Difference bands originate only from those protein residues that are affected by the reaction. All "passive" residues are invisible in the difference spectrum which, therefore, exhibits details of the reaction mechanism on the molecular level despite a large background absorption.

Time-Resolved Infrared Spectroscopy. Several different approaches are available for time-resolved infrared spectroscopy (*1*, *6*, *7*). If sub-nanosecond time resolution is desired, pump−probe techniques have to be used (*12*−*14*). For measurements in the nanosecond to second time range, tunable semiconductor continuous wave infrared lasers supply powerful measuring light sources (*15*). The latter technique reveals dynamic information at single wavelengths only. With Fourier transform spectrometers, millisecond time resolution can be achieved by fast scanning of the movable mirror (rapid scan) (*16*). Iterative recording of time traces at consecutive positions of the mirror (step scan) (*17*) enables nanosecond time resolution but needs approximately 10^5 repetitions of the experiment. Therefore, the reaction under investigation should be highly reproducible. This prerequisite is met for example by the photoreaction of bacteriorhodopsin (see below) or the thermally induced reversible unfolding of a protein. However, the step-scan technique can generally not be applied to nonreproducible reactions.

Techniques for Reaction-Induced Infrared Difference Spectroscopy. The number of methods to initiate protein reactions has constantly increased in the past decade. Now, light-driven reactions, redox reactions, molecule−protein interaction, and protein folding can be studied by infrared spectroscopy. To investigate a given protein reaction, the best suited technique must be chosen. An overview of the currently available methods is given in Table 1. In the following, we describe the techniques and discuss selected examples for illustrative purpose.

Light-Induced Infrared Difference Spectroscopy. Light-induced infrared difference spectroscopy can be used to investigate proteins performing photoreactions, for example the photosynthetic reaction centers from plants or bacteria (*12*, *15*, *18*, *19*) or bacteriorhodopsin (*4*, *5*, *20*). This technique has been applied since the early 1980s and has been the first method among the reaction-induced infrared difference spectroscopy techniques (*21*). The simplest way to acquire difference spectra is to measure the reference in the dark and the sample spectrum under continuous illumination of the sample. In this manner, photostationary states can be accumulated and compared with the ground state. Variation of buffer conditions and temperature has allowed the isolation of intermediate states (*5*). However, often very low temperatures far away from physiological conditions are required to stop the reaction in the desired state. Therefore, it is more elegant (but requires more effort) to use time-resolved techniques with a short light pulse as a trigger of the photoreaction. A reference is measured before the excitation flash, and the photoreaction is followed by time-resolved spectra. By this means, information about the kinetics of the reaction can be obtained in addition to the spectral information.

Bacteriorhodopsin is one of the proteins most intensely studied by infrared spectroscopy (*1*, *3*−*5*). It is a small integral membrane protein which converts light energy into a transmembrane proton gradient (*20*, *22*). Light absorption by the chromophore all-*trans*-retinal starts the photoreaction of bacteriorhodopsin which leads to isomerization of the retinal, changes in secondary structure, and proton transport, involving protonation as well as deprotonation of several groups (including D85, D96, and the Schiff base which links retinal to K216). The photoreaction proceeds via several intermediate states named BR (ground state), J, K, L, M, N, and O. Fortunately, high-resolution structures of the ground state as well as of some intermediate states are available now (see ref *23* and references cited therein). However, many fundamental facts concerning the function of bacteriorhodopsin as a proton pump, namely, the identification of the critical proton donor and acceptor groups and the determination of their protonation state in the different intermediates, have been elucidated several years ago. Since infrared difference spectroscopy is able to directly observe protonation changes of single amino acids, this method played a dominant role in this context (*1*, *3*−*5*).

Table 1: Comparison of Techniques To Initiate Different Kinds of Protein Reactions

technique	light	attenuated total reflection	stopped flow/ continuous flow	temperature jump (laser)	pressure jump	caged compounds	equilibrium electrochemistry	photo-reduction
approximate maximum time resolution	ps−ns depending on the detection method	s−min	50 ms/250 μs	ps−ns depending on the detection method	dead time 20 s	μs−ms depending on the caged compound	equilibration time s−min	in principle fast, presently typically min
minimum amount of protein required	20−100 μg	20−100 μg	> 100 μg/1−2 mg	20−100 μg		20−100 μg	100−500 μg	20−100 μg
comments	chromophore required, laser required	usually a stable protein film is required, buffer easily exchangeable	not for membrane proteins, sample viscosity must be low, temperature jump possible (from cold to hot and vice versa)	temperature-jump decays with ~1−10 ms, only from cold to hot, laser required	special pressure cell required, from high pressure to low pressure and vice versa	only a limited number of cages available, photolysis reaction itself produces infrared signals, UV laser or flash lamp required	no time-resolved measurements, spectroelectrochemical cell required	laser required

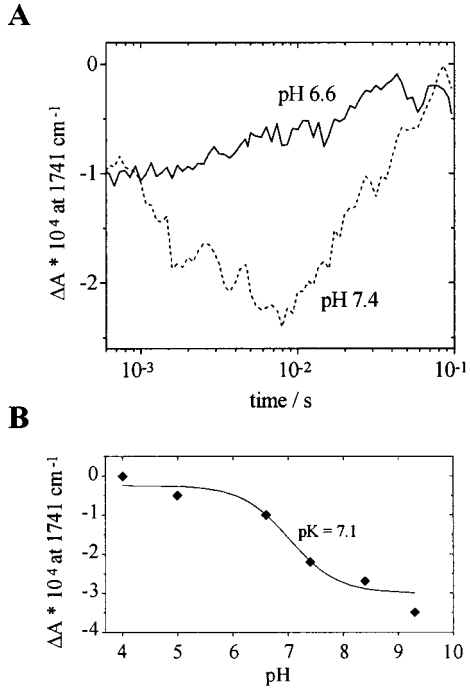

FIGURE 2: (A) Time traces of absorbance changes during the bacteriorhodopsin photoreaction at 1741 cm^{-1} recorded at pH 6.6 (solid line) and pH 7.4 (dashed line), respectively. The negative signal observed at pH 7.4 is attributed to deprotonation of D96 in the N intermediate (C═O stretch of D96). (B) pH dependence of the maximum amplitude of the signal shown in (A). The continuous line represents the fit to the Henderson−Hasselbalch equation. In this way, the pK_a of D96 in the N state was determined to be 7.1 (±0.2).

Essential for an understanding of the proton transport are the pK_a changes of the groups along the proton pathway. For this purpose attenuated total reflection (ATR)[1] (see below) was combined with time-resolved light-triggered difference spectroscopy to enable measurements at well-defined pH[2] (*24*). Applying this technique to bacteriorhodopsin, the pK_a switch of D96 has been investigated (*25*). D96 serves as the proton donor for the Schiff base in the step from M to N (*26*, *27*). Analysis of step-scan measurements at different pH values revealed a pK_a of 7.1 for D96 in the N intermediate (see Figure 2 and ref *25*). For the ground state, ATR experiments can provide only a lower limit for the pK_a of D96 (pK_a = 12)[3] because of sample detachment from the internal reflection element at very high pH (*29*). This limit is 5 units higher than the pK_a of D96 in the N state. The observed pK_a change is an impressive example for the control of the pK_a of an amino acid side chain by the protein environment.

Using the same ATR approach, precise separation of the photointermediates L, M, N, and O was possible by alteration

[1] Abbreviations: ATR, attenuated total reflection; caged ATP, P^3-[1-(2-nitrophenyl)ethyl]adenosine 5'-triphosphate; DM-Nitrophen, 1-(2-nitro-4,5-dimethoxyphenyl)-*N*,*N*,*N*',*N*'-tetrakis[(oxycarbonyl)methyl]-1,2-ethanediamine; EDTA, (ethylenedinitrilo)tetraacetic acid; IRE, internal reflection element; Nitr 5, 1,2-diamino-5-[1-hydroxy-1-(2-nitro-4,5-methylenedioxyphenyl)methyl]phenoxy-2-(2'-amino-5'-methylphenoxy)ethane-*N*,*N*,*N*',*N*'-tetraacetic acid tetrasodium salt.

[2] Preparation of samples for transmission experiments usually involves sample concentration which may change the pH. In contrast, ATR allows to perform infrared spectroscopy in excess water, enabling precise control of the pH.

[3] Solid-state nuclear magnetic resonance experiments proved that D96 is protonated in the ground state up to a pH of 10 (*28*).

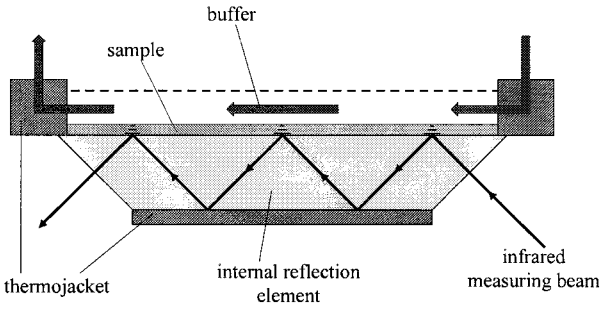

FIGURE 3: Experimental setup for flow attenuated total reflection measurements. The evanescent wave of the infrared beam penetrates the sample which must be in close contact to the surface of the internal reflection element. For simplicity, the number of reflections within the internal reflection element is reduced. A dialysis membrane can be placed above the sample to create a second compartment separated from the sample compartment (*37*). By that means, mechanical perturbations and unintentional concentration changes can be avoided. For illumination of the sample, a fiber bundle can be placed above the ATR accessory (*24*).

of pH and temperature (*30*). In particular, this study led to the first reliable infrared difference spectrum between the O intermediate and the ground state. By that means, it was shown that the acceptor of the Schiff base proton D85 is still protonated in the O intermediate and that the changes in secondary structure which are most pronounced in N are mainly reversed in the N to O reaction.

Introduction to Concentration Jump Techniques. The need to trigger the protein reaction directly in the infrared cuvette is a particular problem when the effect of ions or molecules on proteins is of interest. The small path length of infrared cuvettes makes adding the substrate to a protein sample difficult. Three different approaches have been applied to generate a concentration jump in an infrared sample: (i) the attenuated total reflection (ATR) technique, (ii) the infrared variants of the stopped-flow and continuous-flow techniques, and (iii) the photolytical release of effector substances from biologically "silent" precursors (termed "caged compounds"). Each of the three methods has its specific advantages and drawbacks which are discussed in the following sections (see also Table 1 for a short summary).

Attenuated Total Reflection. Infrared transmission measurements require short optical path lengths (5−10 μm in ^1H_2O, 30−50 μm in ^2H_2O) because of the strong water absorption. Short path lengths in turn lead to high protein concentrations. Direct titration of the sample protein is practically impossible in these cuvettes. An elegant solution of this problem is provided by the ATR technique (*31*−*34*) (see Figure 3). ATR uses the phenomenon of total reflection of electromagnetic waves at interfaces between materials with different refraction indices. Despite the total reflection of the measuring light in the internal reflection element (IRE), absorption by the sample takes place if the sample is in contact with the IRE. This is due to the so-called evanescent wave, which is present in the optically rarer medium. The amplitude of the evanescent wave decreases exponentially with increasing distance z from the interface according to

$$E = E_0 e^{-z/d_p}$$

E_0 is the time-averaged electric field intensity at the interface, in the rarer medium, and E is the time-averaged electric field intensity at the distance z from the interface. The distance d_p, where E is decreased to $1/e$ of E_0, is called depth of penetration. It is related to the angle of incidence θ of the measuring light with respect to the normal of the IRE, to the ratio of the refractive indices ($n_{21} = n_1/n_2$) of the IRE n_1 and the rarer medium n_2, and to the wavelength within the IRE $\lambda_1 = \lambda/n_1$:

$$d_p = \frac{\lambda_1}{2\pi(\sin^2\theta - n_{21}^2)^{1/2}}$$

The larger n_{21}, the shorter λ, and the larger θ are, the shorter is the depth of penetration d_p. Because of the exponential decay of the intensity of the electrical field, a close contact between the sample and the surface of the IRE is essential. In the case of membrane proteins this can usually be achieved by simply drying reconstituted protein or membrane patches on the IRE surface. Subsequently, arbitrary amounts of buffer can be added to the protein−lipid layers. If appropriate conditions are selected, this will result in penetration of the buffer between the layers without detachment of the sample from the IRE. Other methods of preparation are described in refs *32*−*34*. The buffer located above a sufficiently thick sample layer does not contribute to the signal since the intensity of the measuring light is negligible here. The advantage of the ATR technique is that buffer exchange is straightforward. In this way, it is possible to measure difference spectra of membrane proteins that are induced by different buffer conditions (for instance, different pH values or ligand concentrations) and in excess water. Compared to the photolytical variant of concentration-jump-induced infrared difference spectroscopy (see below), the time resolution of the ATR technique is low. However, no chemist has to be asked for the caged version of the substances of interest.

The high potential of the ATR technique to induce protein reactions was demonstrated by Baenziger and co-workers, who studied ligand binding to the nicotinic acetylcholine receptor (*35*, *36*), and by Fahmy, who investigated the influence of binding of transducin and transducin-derived peptides to the rhodopsin photointermediate metarhodopsin II (*37*). An example for the ATR advantage of accurate control of sample conditions (*25*, *30*) has been given in the previous section.

Rapid Mixing Techniques. Although rapid mixing of aqueous solutions is widely used for the analysis of reacting systems by measurements in the UV and visible spectral regions, reports of stopped-flow experiments with detection in the infrared are rare. This is because it is difficult to make a concentrated and thus highly viscous protein solution flow rapidly through the thin slit between the windows of an infrared cuvette. Nevertheless, successful developments of a stopped-flow apparatus for infrared spectroscopy have been reported (*38*, *39*). As the components have to withstand high pressure and since small dead volumes are desired, HPLC technology was used for the interconnections between the conventional pneumatic flow-inducing system and the mixing and cuvette assembly. This system allows rapid mixing of protein solutions with substrate molecules and was used to study deacylation and acylation of chymotrypsin (*38*), binding of carbon monoxide to nitrogenase (*40*), and the interactions between β-lactam antibiotics and β-lactamases (*41*). The latter enzyme is the weapon of some bacteria

against β-lactams which inhibit cell wall synthesis by inactivation of transpeptidase. β-Lactamases are able to destroy these antibiotics by opening of the β-lactam ring. This is achieved by covalently linking the antibiotic to a protein serine residue (acyl enzyme) and concomitant breaking of a C−N bond of the β-lactam ring. Subsequent deacylation by hydrolysis releases the inactive open form of the antibiotic. The active site of the enzyme is supposed to provide two hydrogen bonds to the carbonyl oxygen of β-lactam in order to polarize the carbonyl and aid the hydrolysis reaction of the carbonyl carbon atom. The time-resolved infrared study on the hydrolysis of the β-lactam methicillin by *Citrobacter freudii* β-lactamase (*41*) detected four difference bands which have been assigned to four conformations of the acyl enzyme carbonyl group. Comparison of the bandwidth of these bands (10 cm^{-1}) with the bandwidth of a model ethyl ester in ^2H_2O solution (37 cm^{-1}) denotes a higher degree of ordering of the acyl enzyme conformers. Analysis of the intensities of the difference bands indicates that the conformers are populated approximately proportional to the hydrogen-bonding strength at the carbonyl oxygen. Wilkinson and colleagues suggest that the different conformers reflect different alignments of the substrate in the active site of the protein and thus the lack of specificity. This would not be surprising, since methicillin was designed to frustrate β-lactamase, as far as deacylation is concerned. In addition to bands due to the acyl enzyme carbonyl and the product carboxylate, a difference band at 1628 cm^{-1} was observed. This feature was attributed to a change in the β-sheet structure of the enzyme. From the time dependence of the absorbance differences, it can be concluded that relaxation of the structural change develops simultaneously or slightly faster than formation of the product.

A variant of the stopped-flow technique with improved time resolution is the continuous-flow method (*42*). Very recently, an infrared continuous-flow approach with a time resolution of 250 μs was reported (*43*).

Temperature and Pressure Jump. The stopped-flow technique can also be used to generate a temperature jump (T-jump) for folding and unfolding experiments (*44*, *45*). This approach uses different temperatures in the infrared cell and in the injection syringe initially containing the sample. In this manner, the temperature of the sample may either be increased or decreased depending on the experimental design. Refolding of thermally and chemically unfolded protein was compared by this technique on a time range of 100 ms to minutes (*45*).

Higher time resolution can be achieved in T-jump experiments using a short laser pulse for sample heating. Application of picosecond techniques (*46*, *47*), lead salt infrared diode lasers (*47*, *48*), and step scan (*49*) have been reported. Whereas most of these studies investigated folding of whole proteins, Williams and co-workers used an α-helical alanine-based peptide of 21 residues as a model to examine helix melting and helix formation (*48*). By evaluation of both, the equilibrium constant of the helix−coil transition and the time constant of the T-jump-induced unfolding process, the time constant of the folding event was calculated to be approximately 16 ns for the model peptide.

Analogous to a change in temperature, a change in pressure can initiate folding or unfolding of proteins (*50*). Recently, pressure-jump techniques using infrared detection have been developed for this purpose (*51*).

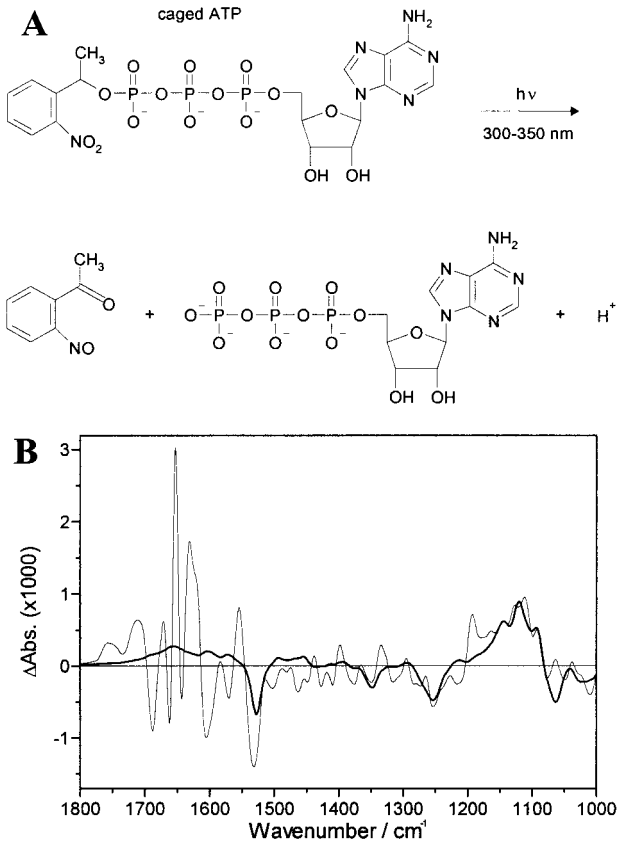

FIGURE 4: (A) Photolysis of caged ATP. (B) Infrared difference spectrum upon release of ATP from caged ATP. Thick line: spectrum of caged ATP photolysis in the absence of protein. Thin line: ATP release in a Ca^{2+}-ATPase sample. Two reactions contribute to the signals: (i) caged ATP photolysis and (ii) the transition of the Ca^{2+}-loaded ATPase to the E_2−P phosphoenzyme where Ca^{2+} has been pumped and released (*87*).

Photolytically Induced Concentration Jump. Caged compounds have been used for 20 years to study biological reactions (*52*). In its caged form, the effector compound is modified such that it does not react with the protein of interest (see Figure 4A for caged ATP). Upon an UV flash (300−350 nm) the caged molecule photolyzes, which leads to a sudden concentration jump of the free effector substance (<10 ms for caged ATP of Figure 4A; other compounds are faster). Effector−substance binding to a protein and subsequent conformational changes alter the infrared spectrum as shown in Figure 4B for ATP release in a Ca^{2+}-ATPase sample (thin line). In addition to protein and effector molecule bands, the photolysis reaction is reflected in the difference spectra. This is shown in Figure 4B, where the thick line represents absorbance changes upon caged ATP photolysis in the absence of protein. The main bands at 1524 and 1342 cm^{-1} have been assigned to the ν_{as} and ν_s stretching vibrations of the nitro group of caged ATP, respectively, and below 1270 cm^{-1} to a diminution of electron density in the phosphate P−O bonds upon photolysis (*53*). Further information can be found in refs *54*−*56*. In infrared studies, caged nucleotides, caged Ca^{2+} (Nitr 5 or DM-Nitrophen), and "caged electrons" (described in the photoreduction section) have been used so far.

The studies undertaken have dealt with two main aspects: (i) molecule−protein recognition and (ii) the molecular basis

of enzyme function. The first aspect involves characterization of molecule binding sites of proteins by infrared spectroscopy and seems to be very promising for future applications. Due to the availability of caged nucleotides, these studies have focused on nucleotide binding to several proteins, reviewed in ref *57*.

Most studies on the molecular basis of enzyme function using the photolytically induced concentration-jump technique have been done on the sarcoplasmic reticulum Ca^{2+}-ATPase (*58*−*62*), which has also been the first enzyme to be studied with this technique (*53*). Further information and references can be found in ref *57*.

Equilibrium Electrochemistry. For the large field of protein-catalyzed redox reactions, infrared investigations became available with the development of an ultrathin-layer spectroelectrochemical cell suitable for protein investigations in aqueous solution (*63*). The spectroelectrochemical cell permits control of the redox state of proteins in the infrared cuvette by applying a potential (E) to a working electrode. According to the Nernst equation

$$E = E_m + \frac{RT}{zF} \ln \frac{[ox]}{[red]}$$

and via electron transfer between electrode and sample, the redox state of the sample adjusts to the applied electrode potential (E_m, midpoint potential of the redox system; R, gas constant; T, temperature; z, charge; F, Faraday constant; [ox] and [red], concentration of the oxidized and reduced species, respectively). By applying a potential step at the working electrode, a redox reaction can be triggered in the electrochemical cell. From the infrared absorbance spectrum before and after the potential step, a difference spectrum can be calculated that reflects only the redox reaction of the protein.

The electrochemical cell is particularly useful when a protein contains several redox-active cofactors with different midpoint potentials as is often the case for proteins involved in photosynthesis and respiration. Since the method allows the accurate control of the sample redox state, it is possible to selectively induce the redox reaction of only one particular cofactor (*64*−*68*), i.e., to "dial a cofactor" (*2*).

As an illustration, a protein with two redox-active cofactors P1 and P2 is considered in Figure 5A, with P2 having the more positive midpoint potential (note that the y axis is inversed in Figure 5A). When the electrode potential is changed, three redox reactions can be triggered, depending on the initial oxidation state of the cofactors and the amplitude of the potential change. These are from left to right in Figure 5A: $P1_{red}P2_{red} \rightleftharpoons P1_{ox}P2_{ox}$, $P1_{red}P2_{red} \rightleftharpoons P1_{ox}P2_{red}$, and $P1_{ox}P2_{red} \rightleftharpoons P1_{ox}P2_{ox}$ and vice versa.

Selective triggering of only one of the possible redox reactions has been achieved for example in studies on the charge separation catalyzed by the bacterial photosynthetic reaction center. It was possible to separate the reaction of the primary electron donor (bacteriochlorophyll dimer) (*66*) from that of the electron acceptor quinone A or B (*67*). In a study of photosystem I, careful experimentation avoided the oxidation of the abundant antenna chlorophylls and allowed the exclusive titration of signals of the primary electron donor P700 (a chlorophyll dimer) (*68*). And, as a final example, it could be shown that Glu 278 of the *Paracoccus denitrificans*

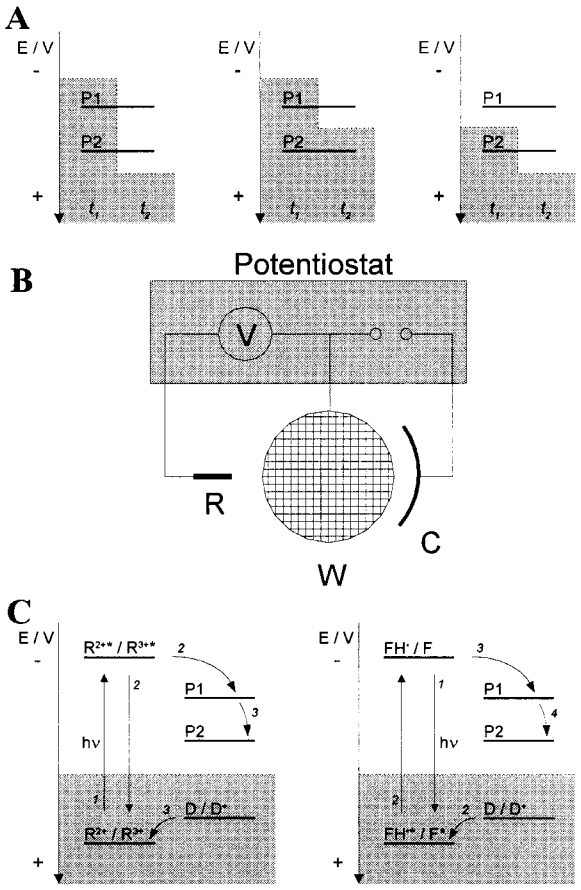

FIGURE 5: Triggering protein redox reactions. (A) Principle of the experiments with the electrochemical cell. Shown are the midpoint potentials of two redox-active protein cofactors P1 and P2 (full lines), with that of P2 being more positive than P1 (note that the y axis is inverted). The dotted borderline between the gray and white area indicates the potential of the working electrode which is switched, for example, from a reducing potential at time t_1 to an oxidizing potential at time t_2 in the experiment. The figure is arranged such that cofactors are reduced when they lie within the gray area at t_1 and/or t_2. Left: At t_1 the electrode potential is more negative than the midpoint potential of both cofactors P1 and P2. Thus they are both reduced at the beginning of the experiment. After the potential step at t_2, the electrode potential is more positive than both midpoint potentials and both cofactors are oxidized. Thus the potential step has triggered the full oxidation: $P1_{red}P2_{red} \rightarrow P1_{ox}P2_{ox}$. Middle: Both cofactors are reduced at t_1. Compared to the previous case, the potential step applied is smaller and only P1 is oxidized at t_2 while P2 remains reduced. The potential step has thus selectively oxidized P1: $P1_{red}P2_{red} \rightarrow P1_{ox}P2_{red}$. Right: The working electrode potential is chosen such that P1 is oxidized at the beginning of the experiment and P2 is reduced. After the potential step, P2 is oxidized too. This time, the potential step has selectively oxidized P2: $P1_{ox}P2_{red} \rightarrow P1_{ox}P2_{ox}$. Of course, in the above examples the back-reactions can be triggered by reversing the potential steps applied. (B) Electrode arrangement of the electrochemical cell with working electrode W, counter electrode C, and reference electrode R. Two CaF_2 windows above and below the working electrode close the cell. The measuring light beam is perpendicular to the paper plane and passes through the gold net that constitutes the working electrode. (C) Photoreduction of proteins. Shown are the midpoint potentials of two protein cofactors, P1 and P2, of the sacrificial electron donor EDTA D, of the ruthenium complex R (left), and of flavin F (right). The dotted, horizontal line indicates the equilibrium sample potential. Species with a more positive midpoint potential than the sample potential are in the reduced state and located in the gray area of the figure. Vertical transitions occur between the two midpoint potentials of the photoexcitable system; curved arrows indicate electron transfer. The numbers show the sequence of events.

cytochrome *c* oxidase is involved in the redox reaction of heme *a* (and possibly Cu_B) (*65*).

The infrared electrochemical cell has the typical three-electrode arrangement shown in Figure 5B with a working electrode, a counter electrode, and the reference electrode. A 55−70% transparent, 6 μm thick gold grid serves as the working electrode. It lies on one of the two CaF_2 windows that build up the infrared cuvette. The gold grid is usually coated with a modifier that prevents irreversible adsorption of proteins onto the gold surface. The working electrode potential is measured against a Ag/AgCl reference electrode and is set to the desired value by a potentiostat. Because of the high resistance of the potentiostat voltmeter, the current between the working electrode and reference electrode is very small. The main current flows between the working electrode and the counter electrode, which consists of a platinum foil in electrical contact to the sample but outside the measuring light beam. The arrangement of electrodes ensures that the sample in the measuring light beam adopts the potential of the working electrode, i.e., that only the desired reactions are monitored. Reactions that take place at the counter electrode are outside the measuring light beam.

The total path length of the cuvette is about 10 μm, which is advantageous since it ensures relatively fast equilibration of the sample after a potential step at the working electrode. The CaF_2 window material is transparent from 200 nm to 10 μm and allows simultaneous control measurements in the visible spectral region concomitant to the infrared measurements. In addition to the spectral information, the signals can be titrated against the applied potential in order to determine the midpoint potentials of the cofactors.

In a typical experiment, the protein is first equilibrated at a certain electrode potential; then the potential at the working electrode is altered, for example, decreased. This is transmitted to the protein molecules via small mediator molecules that each pick up an electron from the electrode, diffuse to a protein molecule, reduce it, and diffuse back to the electrode. Usually within seconds to minutes, the redox state of the protein has adjusted to the new potential at the working electrode. When the potential range used in the experiment is large, a mediator "cocktail" has to be used where the midpoint potentials of the different mediator molecules cover the potential range of the experiment (*65*, *69*−*71*). The redox reactions of the mediator molecules are practically invisible in the infrared difference spectrum because of their small concentration. However, they induce buffer protonation or deprotonation, which gives rise to infrared difference signals.

Without mediator molecules, equilibration is often very slow because of the slow diffusion of protein molecules and because of slow electron transfer from the electrode to the redox-active centers which can be buried in the protein. Some proteins such as cytochrome *c* (*63*), however, equilibrate fast even without mediators. Then the equilibration time depends on the modification of the electrode (*72*, *73*). For efficient electron transfer in the absence of mediators, the redox-active center must be easily accessible for electron transfer from the electrode. The equilibration time in the absence of mediators is thus a measure for the accessibility of the redox-active cofactors (*74*).

While recent work with the infrared electrochemical cell has concentrated on cytochrome *c* oxidases (*65*, *70*, *75*, *76*), many of the original publications were devoted to photosynthesis (*66*−*68*). They nicely illustrate how this approach provides information on the protein environment of the redox-active cofactors. In photosystems I and II of cyanobacteria and plants and in reaction centers of purple bacteria, light is absorbed by the primary electron donor, which is composed of two chlorophyll *a* or two bacteriochlorophyll molecules, respectively. This produces the highly reducing excited state and initiates electron transfer from the primary donor via a chain of cofactors to the electron acceptors. The difference spectra of light-induced charge separation of the bacterial reaction centers of *Rhodobacter sphaeroides* and *Rhodopseudomonas viridis* are largely dominated by the oxidation of the primary donor (*66*) with prominent contributions from the bacteriochlorophyll dimer itself. Interestingly, there is also evidence for the involvement of a water molecule in this reaction (for *Rb. sphaeroides*) (*66*). Extensive model studies of the isolated cofactor redox reactions in different solvents (*77*−*79*) allowed the assignment of signals in the protein spectra to specific molecular groups of the cofactors. By comparison of different purple bacteria (*Rb. sphaeroides* and *Rp. viridis*) (*66*) and photosystem I (of *Synechocystis* PCC 6803) (*68*), subtle differences were found for the H-bonding pattern to the two chlorophyll *a* or bacteriochlorophyll molecules that constitute the primary donor. For photosystem I, the two chlorophyll *a* molecules have a different protein environment. Monomeric chlorophyll is a good model for the difference spectrum of primary donor oxidation, which shows that the charge of the oxidized donor is localized on only one of the two molecules (*68*). This is in contrast to the bacterial reaction centers investigated (*66*), where the charge is delocalized on both of the bacteriochlorophyll molecules. These detailed investigations of cofactor environment were only possible because signals of protein backbone perturbations were rather small (*6*, *19*), indicating that the protein rather provides an "optimized solvent" (*6*) than acts via considerable conformational changes. Further information on vibrational spectroscopy of reaction centers can be found in refs *18*, *19*, and *80*.

Photoreduction. Recently, a second method has entered infrared spectroscopy of redox reactions. It is based on photoexcitable electron donors such as riboflavin or Ru^{2+} complexes for which the expression "caged electron" has been coined (*81*). Light absorption and electron transfer shuttle these systems between a highly oxidizing and a highly reducing state. Figure 5C shows a scheme of the midpoint potentials, with the vertical arrows indicating the transitions between these two redox states. The principle is similar to that of photosynthetic reaction centers where photoexcitation of the primary donor produces a highly reducing excited state and initiates electron-transfer reactions within the protein.

In the case of tris(2,2'-bipyridyl)ruthenium(II) (R^{2+}), photoreduction of a protein (P) proceeds according to the scheme (*82*)

$$R^{2+} \rightarrow R^{2+}*$$

$$R^{2+}* + P_{ox} \rightarrow R^{3+} + P_{red}$$

$$R^{3+} + D \rightarrow R^{2+} + D^{+}$$

Photoexcitation directly produces the strongly reducing excited state ($R^{2+}*$) which transfers one electron to the protein. The product (R^{3+}) irreversibly oxidizes the sacrificial

electron donor EDTA (D), which re-forms the initially reduced ruthenium complex (R^{2+}) (*82*). The irreversibility of EDTA oxidation prevents that oxidized EDTA is finally reduced by the protein and thus enables the accumulation of the reduced protein state.

The mechanism is more complicated in the case of flavins (*83*) because the reduced form that is capable of donating electrons to protein cofactors has first to be generated:

$$F + h\nu \rightarrow F^*$$

$$F^* + DH_2 \rightarrow FH^\bullet + DH^\bullet \quad \text{or} \quad F^* + P_{red} \rightarrow F^{\bullet -} + P_{ox} \quad \text{(photooxidation)}$$

$$FH^\bullet + P_{ox} \rightarrow F + P_{red} + H^+ \quad \text{(photoreduction)}$$

Photoexcitation of flavin (F) generates the triplet state (F*) with high quantum efficiency. In contrast to the previous case, this excited state is a strong oxidant which may directly be used to oxidize proteins (*83*). However, there is also the possibility to produce a strong reductant—the flavin semiquinone ($FH^\bullet$)—by irreversible oxidation of the sacrificial donor EDTA (DH_2). The flavin semiquinone is able to reduce protein cofactors ($P1_{ox}$), and this has been used in most of the infrared studies.

In a protein with two redox-active cofactors, P1 and P2, with P2 having the more positive midpoint potential (see Figure 5C), single electron transfer reduces only P2 and thus triggers the reaction $P1_{ox}P2_{ox} \rightarrow P1_{ox}P2_{red}$. The transfer of two electrons leads to the fully reduced protein $P1_{red}P2_{red}$ from initially $P1_{ox}P2_{ox}$. If the redox potential of the sample is adjusted such that $P2_{red}$ is produced at the beginning of the experiment, then photoexcitation triggers the single electron-transfer reaction $P1_{ox}P2_{red} \rightarrow P1_{red}P2_{red}$. In principle, therefore, the same redox transitions can be triggered with photoreduction and with equilibrium electrochemistry.

Photoreduction-induced infrared difference spectroscopy has been successfully employed in studies of aa_3 cytochrome *c* oxidase of *Rb. sphaeroides*, bo_3 (*81*, *84*, *85*) and *bd* (*86*) ubiquinol oxidases of *Escherichia coli*, and cytochrome $P\text{-}450_{cam}$ (*82*). The method is an interesting complement to the electrochemical cell since, in principle, it allows time-resolved measurements (*82*). The spectra obtained by protein photoreduction closely resemble those obtained with the electrochemical cell for cytochrome *c* (*81*) and for two related aa_3 cytochrome *c* oxidases (*75*, *81*), although contributions from the oxidation of the sacrificial electron donor EDTA would be expected.

Conclusions. In summary, it may be said that reaction-induced infrared difference spectroscopy allows sensitive and specific detection of structural differences between a protein in state A and state B. Structural changes of conformationally active regions of the protein backbone as well as subtle changes concerning single amino acid side chains are reflected in the difference spectra. The reaction between the two states may be triggered by a change in the concentration of a chemical compound, by the absorption of light, by a temperature or pressure jump, or by a change in the potential. The diversity of the methods enables various problems to be addressed. Progress in the development of new techniques may even expand the range of applications and the sensitivity of the method. Nonetheless, infrared difference spectroscopy was already able to significantly promote research in such different fields as bioenergetics, protein folding, and molecule−protein recognition.

ACKNOWLEDGMENT

We are indebted to W. Mäntele for his continuous support. P. Hellwig is acknowledged for critical reading of the manuscript. We would like to apologize to our colleagues whose publications could not be cited because of limitations of space.

REFERENCES

1. Siebert, F. (1995) *Methods Enzymol. 246*, 501−526.
2. Mäntele, W. (1993) *Trends Biochem. Sci.*, 197−202.
3. Gerwert, K. (1999) *Biol. Chem. 380*, 931−935.
4. Rothschild, K. J. (1992) *J. Bioenerg. Biomembr. 24*, 147−167.
5. Maeda, A. (1995) *Isr. J. Chem. 35*, 387−400.
6. Mäntele, W. (1996) in *Biophysical techniques in photosynthesis* (Amesz, J., Ed.) pp 137−160, Kluwer Academic Publishers, Dordrecht.
7. Slayton, R. M., and Anfinrud, P. A. (1997) *Curr. Opin. Struct. Biol. 7*, 717−721.
8. Barth, A. (2000) *Prog. Biophys. Mol. Biol.* (in press).
9. Kauppinen, J. K., Moffatt, D. J., Mantsch, H. H., and Cameron, D. G. (1981) *Appl. Spectrosc. 35*, 271−276.
10. Mantsch, H. H., Moffatt, D. J., and Casal, H. L. (1988) *J. Mol. Struct. 173*, 285−298.
11. Barth, A. (2000) *Spectrochim. Acta A 56*, 1223−1232.
12. Hamm, P., Zurek, M., Mäntele, W., Meyer, M., Scheer, H., and Zinth, W. (1995) *Proc. Natl. Acad. Sci. U.S.A. 92*, 1826−1830.
13. Diller, R., Iannone, M., Cowen, B. R., Maiti, S., Bogomolni, R., and Hochstrasser, R. M. (1992) *Biochemistry 31*, 5567−5572.
14. Lim, M., Jackson, T. A., and Anfinrud, P. A. (1997) *Nat. Struct. Biol. 4*, 209−214.
15. Mäntele, W., Hienerwadel, R., Lenz, F., Riedel, W. J., Grisar, R., and Tacke, M. (1990) *Spectrosc. Int. 2*, 29−35.
16. Braiman, M. S., Ahl, P. L., and Rothschild, K. J. (1987) *Proc. Natl. Acad. Sci. U.S.A. 84*, 5221−5225.
17. Uhmann, W., Becker, A., Taran, C., and Siebert, F. (1991) *Appl. Spectrosc. 45*, 390−397.
18. Nabedryk, E. (1996) in *Infrared spectroscopy of biomolecules* (Mantsch, H. H., Ed.) pp 39−82, Wiley-Liss, New York.
19. Mäntele, W. (1993) in *The photosynthetic reaction center* (Deisenhofer, J., Ed.) pp 239−283, Academic Press, San Diego.
20. Heberle, J., Fitter, J., Sass, H. J., and Büldt, G. (2000) *Biophys. Chem. 85*, 229−248.
21. Siebert, F., Mäntele, W., and Kreutz, W. (1980) *Biophys. Struct. Mech. 6*, 139−146.
22. Lanyi, J. K. (2000) *Biochim. Biophys. Acta 1459*, 339−345.
23. Kühlbrandt, W. (2000) *Nature 406*, 569−570.
24. Heberle, J., and Zscherp, C. (1996) *Appl. Spectrosc. 50*, 588−596.
25. Zscherp, C., Schlesinger, R., Tittor, J., Oesterhelt, D., and Heberle, J. (1999) *Proc. Natl. Acad. Sci. U.S.A. 96*, 5498−5503.
26. Butt, H. J., Fendler, K., Bamberg, E., Tittor, J., and Oesterhelt, D. (1989) *EMBO J. 8*, 1657−1663.
27. Gerwert, K., Souvignier, G., and Hess, B. (1990) *Proc. Natl. Acad. Sci. U.S.A. 87*, 9774−9778.
28. Metz, G., Siebert, F., and Engelhard, M. (1992) *Biochemistry 31*, 455−462.
29. Zscherp, C. (1997) Der Protonentransport durch das Membranprotein Bacteriorhodopsin, untersucht mittels zeitaufgelöster Infrarotspektroskopie (182), pp 1−113, Jülich, Forschungszentrum Jülich GmbH, Berichte des Forschungszentrums Jülich.
30. Zscherp, C., and Heberle, J. (1997) *J. Phys. Chem. B 101*, 10542−10547.

31. Harrick, N. J. (1979) in *Internal Reflection Spectroscopy*, Harrick Scientific Corp., Ossining, NY.
32. Tamm, L. K., and Tatulian, S. A. (1997) *Q. Rev. Biophys. 30*, 365−429.
33. Fringeli, U. P., Goette, J., Reiter, G., Siam, M., and Baurecht, D. (1998) Structural Investigations of Oriented Membrane Assemblies by FTIR-ATR Spectroscopy (de Haseth, J. A., Ed.) Proceedings of the 11th International Conference on Fourier Transform Spectroscopy (430), Woodbury, NY, The American Institute of Physics, AIP Conference Proceedings.
34. Goormaghtigh, E., Raussens, V., and Ruysschaert, J.-M. (1999) *Biochim. Biophys. Acta 1422*, 105−185.
35. Baenziger, J. E., Miller, K. W., and Rothschild, K. J. (1992) *Biophys. J. 61*, 983−992.
36. Baenziger, J. E., and Chew, J. P. (1997) *Biochemistry 36*, 3617−3624.
37. Fahmy, K. (1998) *Biophys. J. 75*, 1306−1318.
38. White, A. J., Drabble, K., and Wharton, C. W. (1995) *Biochem. J. 306*, 843−849.
39. Masuch, R., and Moss, D. A. (1999) in *Spectroscopy of Biological Molecules: New Directions* (Greve, J., Puppels, G. J., and Otto, C., Eds.) pp 689−690, Kluver Academic Publishers, Dordrecht.
40. George, S. J., Ashby, G. A., Wharton, C. W., and Thorneley, R. N. F. (1997) *J. Am. Chem. Soc. 119*, 6450−6451.
41. Wilkinson, A.-S., Ward, S., Kania, M., Page, M. G. P., and Wharton, C. W. (1999) *Biochemistry 38*, 3851−3856.
42. Shastry, M. C. R., Luck, S. D., and Roder, H. (1998) *Biophys. J. 74*, 2714−2721.
43. Kauffmann, E., Darnton, N. C., Austin, R. H., and Gerwert, K. (2000) *Eur. Biophys. J. 29*, 271−271.
44. Backmann, J., Fabian, H., and Naumann, D. (1995) *FEBS Lett. 364*, 175−178.
45. Reinstädler, D., Fabian, H., Backmann, J., and Naumann, D. (1996) *Biochemistry 35*, 15822−15830.
46. Phillips, G. N., Jr., and Pettitt, B. M. (1995) *Protein Sci. 4*, 149−158.
47. Dyer, R. B., Gai, F., Woodruff, W. H., Gilmanshin, R., and Callender, R. H. (1998) *Acc. Chem. Res. 31*, 709−716.
48. Williams, S., Causgrove, T. P., Gilmanshin, R., Fang, K. S., Callender, R. H., Woodruff, W. H., and Dyer, R. B. (1996) *Biochemistry 35*, 691−697.
49. Wang, J., and El-Sayed, M. A. (1999) *Biophys. J. 76*, 2777−2783.
50. Wong, P. T., and Heremans, K. (1988) *Biochim. Biophys. Acta 956*, 1−9.
51. Panick, G., Malessa, R., Winter, R., Rapp, G., Frye, K. J., and Royer, C. A. (1998) *J. Mol. Biol. 275*, 389−402.
52. Corrie, J. E., and Trentham, D. R. (1993) in *Bioorganic Photochemistry* (Morrison, H., Ed.) pp 243−305, John Wiley & Sons, New York.
53. Barth, A., Mäntele, W., and Kreutz, W. (1990) *FEBS Lett. 277*, 147−150.
54. Barth, A., Hauser, K., Mäntele, W., Corrie, J. E., and Trentham, D. R. (1995) *J. Am. Chem. Soc. 117*, 10311−10316.
55. Barth, A., Corrie, J. E., Gradwell, M. J., Maeda, Y., Mäntele, W., Meier, T., and Trentham, D. R. (1997) *J. Am. Chem. Soc. 119*, 4149−4159.
56. Cepus, V., Ulbrich, C., Allin, C., Troullier, A., and Gerwert, K. (1998) *Methods Enzymol. 291*, 223−245.
57. Barth, A., and Zscherp, C. (2000) *FEBS Lett. 477*, 151−156.
58. Barth, A. (1999) *J. Biol. Chem. 274*, 22170−22175.
59. Barth, A., and Mäntele, W. (1998) *Biophys. J. 75*, 538−544.
60. Georg, H., Barth, A., Kreutz, W., Siebert, F., and Mäntele, W. (1994) *Biochim. Biophys. Acta 1188*, 139−150.
61. Buchet, R., Jona, I., and Martonosi, A. (1991) *Biochim. Biophys. Acta 1069*, 209−217.
62. Troullier, A., Gerwert, K., and Dupont, Y. (1996) *Biophys. J. 71*, 2970−2983.
63. Moss, D., Nabedryk, E., Breton, J., and Mäntele, W. (1990) *Eur. J. Biochem. 187*, 565−572.
64. Hellwig, P., Soulimane, T., Buse, G., and Mäntele, W. (1999) *Biochemistry 38*, 9648−9658.
65. Hellwig, P., Behr, J., Ostermeier, C., Richter, O. M., Pfitzner, U., Odenwald, A., Ludwig, B., Michel, H., and Mäntele, W. (1998) *Biochemistry 37*, 7390−7399.
66. Leonhard, M., and Mäntele, W. (1993) *Biochemistry 32*, 4532−4538.
67. Bauscher, M., Leonhard, M., Moss, D. A., and Mäntele, W. (1993) *Biochim. Biophys. Acta 1183*, 59−71.
68. Hamacher, E., Kruip, J., Rögner, M., and Mäntele, W. (1996) *Spectrochim. Acta A 52*, 107−121.
69. Baymann, F., Moss, D. A., and Mäntele, W. (1991) *Anal. Biochem. 199*, 269−274.
70. Dodson, E. D., Zhao, X. J., Caughey, W. S., and Elliott, C. M. (1996) *Biochemistry 35*, 444−452.
71. De Lacey, A. L., Hatchikian, E. C., Volbeda, A., Frey, M., Fontecilla-Camps, J. C., and Fernandez, V. M. (1997) *J. Am. Chem. Soc. 119*, 7181−7189.
72. Schlereth, D. D., and Mäntele, W. (1992) *Biochemistry 31*, 7494−7502.
73. Schlereth, D. D., and Mäntele, W. (1993) *Biochemistry 32*, 1118−1126.
74. Baymann, F., Robertson, D. E., Dutton, P. L., and Mäntele, W. (1999) *Biochemistry 38*, 13188−13199.
75. Hellwig, P., Rost, B., Kaiser, U., Ostermeier, C., Michel, H., and Mäntele, W. (1996) *FEBS Lett. 385*, 53−57.
76. Behr, J., Michel, H., Mäntele, W., and Hellwig, P. (2000) *Biochemistry 39*, 1356−1363.
77. Mäntele, W. G., Wollenweber, A. M., Nabedryk, E., and Breton, J. (1988) *Proc. Natl. Acad. Sci. U.S.A. 85*, 8468−8472.
78. Bauscher, M., and Mäntele, W. (1992) *J. Phys. Chem. 96*, 11101−11108.
79. Nabedryk, E., Leonhard, M., Mäntele, W., and Breton, J. (1990) *Biochemistry 29*, 3242−3247.
80. Mäntele, W. (1995) in *Anoxygenic Photosynthetic Bacteria* (Blankenship, E., Ed.) pp 627−647, Kluwer Academic Publishers, Dordrecht.
81. Lübben, M., and Gerwert, K. (1996) *FEBS Lett. 397*, 303−307.
82. Contzen, J., and Jung, C. (1999) *Biochemistry 38*, 16253−16260.
83. Tollin, G. (1995) *J. Bioenerg. Biomembr. 27*, 303−309.
84. Lübben, M., Prutsch, A., Mamat, B., and Gerwert, K. (1999) *Biochemistry 38*, 2048−2056.
85. Yamazaki, Y., Kandori, H., and Mogi, T. (1999) *J. Biochem. 126*, 194−199.
86. Yamazaki, Y., Kandori, H., and Mogi, T. (1999) *J. Biochem. 125*, 1131−1136.
87. Barth, A., von Germar, F., Kreutz, W., and Mäntele, W. (1996) *J. Biol. Chem. 271*, 30637−30646.

BI002567Y